Implications from $B \to K^*\ell^+\ell^-$ observables using $3\,\text{fb}^{-1}$ of LHCb data.

Rusa Mandal* and Rahul Sinha†
The Institute of Mathematical Sciences, Taramani, Chennai 600113, India
and
Homi Bhabha National Institute Training School Complex, Anushakti Nagar, Mumbai 400085, India
(Dated: January 30, 2017)

The decay mode $B \to K^*\ell^+\ell^-$ results in the measurement of a large number of related observables by studying the angular distribution of the decay products and is regarded as a sensitive probe of physics beyond the standard model (SM). Recently, LHCb has measured several of these observables using $3\,\text{fb}^{-1}$ data, as a binned function of q^2, the dilepton invariant mass squared. We show how data can be used without any approximations to extract theoretical parameters describing the decay and to obtain a relation amongst observables within the SM. We find three kinds of significant disagreement between theoretical expectations and values obtained by fits. The values of the form factors obtained from experimental data show significant discrepancies when compared with theoretical expectations in several q^2 bins. We emphasize that this discrepancy cannot arise completely due to resonances and non-factorizable contributions from charm loops. Further, a relation between form factors expected to hold at large q^2 is very significantly violated. Finally, the relation between observables also indicates some deviations in the forward-backward asymmetry in the same q^2 regions. These discrepancies are possible evidence of physics beyond the SM.

PACS numbers: 11.30.Er,13.25.Hw, 12.60.-i

I. INTRODUCTION

The rare decay $B \to K^*\ell^+\ell^-$ involves a $b \to s$ flavor changing loop induced transition at the quark level making it attractive mode to search for physics beyond the standard model (SM). Indirect searches for new physics (NP) involving loop processes require a comparison of theoretical estimates with experimental observations. The theoretical estimates thus need to be extremely reliable in order to make a conclusive claim on the existence or non-existence of NP. Fortunately, significant progress has been made in understanding the hadronic effects involved in the decay $B \to K^*\ell^+\ell^-$. The mode $B \to K^*\ell^+\ell^-$ is also of special interest as it allows for the measurement of several observables using the angular distribution [1]. The large number of observables depend on theoretical parameters that describe this decay. In this paper we show how some of the parameters can be extracted directly from LHCb measurements allowing us to verify our theoretical understanding. Any discrepancy observed must be attributed either to a failure of our understanding of hadronic effects or to the existence of NP. We also test the relation between observables that provides another clean test for NP.

The differential decay distribution [1–3] of $B \to K^*\ell^+\ell^-$ results in the measurement of at least nine observables using the angular distribution, as a function of q^2 the dilepton invariant mass squared. These observables are commonly chosen to be the differential decay rate with respect to q^2, two independent helicity fractions that describe the decay, the three asymmetries that describe the real part of the interference between different helicity amplitudes and three asymmetries that describe the imaginary part of the interference.

Recently LHCb [4] has reported measurements of all these observables that have been averaged in eight q^2 bins. A lot of studies on this decay mode are widely discussed in literature [5, 6]. We use the LHCb data to obtain estimates of hadronic form factors that describe the decay. Previously some of the form factors have been determined [7] using $1\,\text{fb}^{-1}$ of LHCb data. We emphasize that our approach does not involve evaluating the decay amplitude in terms of theoretically estimated parameters. Instead we start with the most general parametric form of the amplitude without any hadronic approximations within the SM (see Eq. (5) below). Experimental data alone is used to fit the theoretical parameters introduced in the parametric amplitude. These experimentally fitted theoretical parameters are simply compared to the estimates by other authors [10, 14] which are widely regarded as the state of the art. The values of form factors obtained from experimental data show significant discrepancy when compared with theoretical expectations in several q^2 bins.

In addition to extracting form factors from data, this mode also allows a relation among observables that can provide a clean signal [2, 3] of NP. We find that the measurements do not satisfy the expected relation between the observables in the same q^2 domains where the fitted form factors also show a large discrepancy with the theoretical estimates. The simultaneous observation of these discrepancies points to possible evidence of NP.

The paper is organized as follows. In Sec. II we de-

* rusam@imsc.res.in
† sinha@imsc.res.in

scribe the theoretical framework developed to write the most general parametric form of the amplitude and cast the observables in a form where hadronic paremeters can be obtainable from data. The relation among observables are also derived here. A numerical analysis is presented in Sec. III which contains two subsections. The Sub-sec. III A gives elaborate description of extraction of form factors using LHCb measurements, whereas, the validity of the relations derived assuming SM are examined in Sub-sec. III B with experimental data. In Sec. IV we summarize the important results obtained in this paper. Appendix. A and B estimate the complex part the amplitude and the systematic uncertainty arising mainly due to bin average effect of the observables, respectively.

II. OBSERVABLES AND THEORETICAL FRAMEWORK

In this section we briefly discuss the theoretical framework derived to take into account all possible contributions within SM for the decay $B \to K^*\ell^+\ell^-$. We start with the observables as defined in Ref. [2] to be the F_L, $F_\perp$, A_4, A_5, $A_{\rm FB}$, A_7, A_8, A_9 and $d\Gamma/dq^2 \equiv \Gamma_f$. The observables $F_\perp$, A_4, A_5, $A_{\rm FB}$, A_7, A_8 and A_9 are related to the CP averaged observables S_3, S_4, S_5, $A_{\rm FB}^{\rm LHCb}$, S_7, S_8 and S_9 measured by LHCb [4, 8] as follows:

$$F_\perp = \frac{1-F_L+2S_3}{2}, \quad A_4 = -\frac{2}{\pi}S_4, \quad A_5 = \frac{3}{4}S_5,$$
$$A_{\rm FB} = -A_{\rm FB}^{\rm LHCb}, \; A_7 = \frac{3}{4}S_7, \; A_8 = -\frac{2}{\pi}S_8, \; A_9 = \frac{3}{2\pi}S_9. \quad (1)$$

It may be remarked that LHCb collaboration observes a local tension with some observables based on the hadronic estimates of Refs. [10, 11].

We begin by assuming the massless lepton limit but generalize to include the lepton mass. The corrections due to the mass of the leptons are easily taken into account [2]. In the massless lepton limit the decay is described in terms of six transversity amplitudes which can be written in the most general form as,

$$\mathcal{A}_\lambda^{L,R} = C_{L,R}^\lambda \mathcal{F}_\lambda - \widetilde{\mathcal{G}}_\lambda = (\widetilde{C}_9^\lambda \mp C_{10})\mathcal{F}_\lambda - \widetilde{\mathcal{G}}_\lambda. \quad (2)$$

This form of the amplitude [2] is the most general parametric form of SM amplitude for $B \to K^*\ell^+\ell^-$ decay that comprehensively takes into account all contributions up to $\mathcal{O}(G_F)$ within it. The form includes all short-distance and long-distance effects, factorizable and nonfactorizable contributions and resonance contributions. In Eq. (2) C_9 and C_{10} are Wilson coefficients with $\widetilde{C}_9^\lambda$ being the redefined "effective" Wilson coefficient defined [2, 12] such that

$$\widetilde{C}_9^\lambda = C_9 + \Delta C_9^{\rm (fac)}(q^2) + \Delta C_9^{\lambda,{\rm (non\text{-}fac)}}(q^2) \quad (3)$$

where $\Delta C_9^{\rm (fac)}(q^2)$, $\Delta C_9^{\lambda,{\rm (non\text{-}fac)}}(q^2)$ correspond to factorizable and soft gluon non-factorizable contributions. Strong interaction effects coming from electromagnetic corrections to hadronic operators do not affect C_{10}.

The form factors $\mathcal{F}_\lambda$ and $\widetilde{\mathcal{G}}_\lambda$ introduced in Eq. (2) can be related to the conventional form factors describing the decay as shown in the appendix of Ref. [2]. The form-factors $\mathcal{F}_\lambda$ are of particular interest here as we show that they can be extracted directly from data. The $\mathcal{F}_\lambda$ can be related to the well known form-factors V, A_1 and A_{12} by comparing with [10]:

$$\mathcal{F}_\perp = N\sqrt{2}\sqrt{\lambda(m_B^2, m_{K^*}^2, q^2)}\frac{V(q^2)}{m_B + m_{K^*}}, \quad (4a)$$
$$\mathcal{F}_\parallel = -N\sqrt{2}(m_B + m_{K^*})A_1(q^2), \quad (4b)$$
$$\mathcal{F}_0 = \frac{-N}{\sqrt{q^2}}\, 8 m_B m_{K^*} A_{12}(q^2). \quad (4c)$$

It should be noted that $\mathcal{F}_\lambda$'s and C_{10} are completely real in the SM, with all imaginary contributions to the amplitude arising only from the imaginary part of complex $\widetilde{C}_9^\lambda$ and $\widetilde{\mathcal{G}}_\lambda$ terms. Thus with the introduction of two variables r_λ and ε_λ the amplitude $\mathcal{A}_\lambda^{L,R}$ in Eq. (2) can be rewritten as,

$$\mathcal{A}_\lambda^{L,R} = (\mp C_{10} - r_\lambda)\mathcal{F}_\lambda + i\varepsilon_\lambda, \quad (5)$$

where,

$$r_\lambda = \frac{{\rm Re}(\widetilde{\mathcal{G}}_\lambda)}{\mathcal{F}_\lambda} - {\rm Re}(\widetilde{C}_9^\lambda), \quad (6)$$
$$\varepsilon_\lambda = {\rm Im}(\widetilde{C}_9^\lambda)\mathcal{F}_\lambda - {\rm Im}(\widetilde{\mathcal{G}}_\lambda). \quad (7)$$

The imaginary contributions arise mostly from resonant long-distance contributions, which can be removed by studying only those q^2 regions where no resonances can contribute. In practice this means the removal of charmonium resonance regions from the whole q^2 range. LHCb $3\,{\rm fb}^{-1}$ measurements [4] conservatively exclude the resonance region. Moreover, the contributions from imaginary parts are bounded directly from the LHCb measurements and the bin average values of the ε_λ's are found to be very small as shown in Appendix. A. Hence for now we are neglecting the ε_λ's and will address it's contribution in the numerical analysis.

It is convenient to define P_1 and P_2 as,

$$\mathsf{P}_1 = \frac{\mathcal{F}_\perp}{\mathcal{F}_\parallel}, \qquad \mathsf{P}_2 = \frac{\mathcal{F}_\perp}{\mathcal{F}_0}. \quad (8)$$

The observables $F_\perp$, F_L, $A_{\rm FB}$, A_5 and A_4 can be written [2] as

$$F_\perp = u_\perp^2 + 2\zeta \quad (9)$$
$$F_L\mathsf{P}_2^2 = u_0^2 + 2\zeta \quad (10)$$
$$A_{\rm FB}^2 = \frac{9\zeta}{2\mathsf{P}_1^2}\left(u_\parallel \pm u_\perp\right)^2 \quad (11)$$
$$A_5^2 = \frac{9\zeta}{4\mathsf{P}_2^2}\left(u_0 \pm u_\perp\right)^2 \quad (12)$$
$$A_4 = \frac{\sqrt{2}}{\pi\mathsf{P}_1\mathsf{P}_2}\left(2\zeta \pm u_0 u_\parallel\right) \quad (13)$$

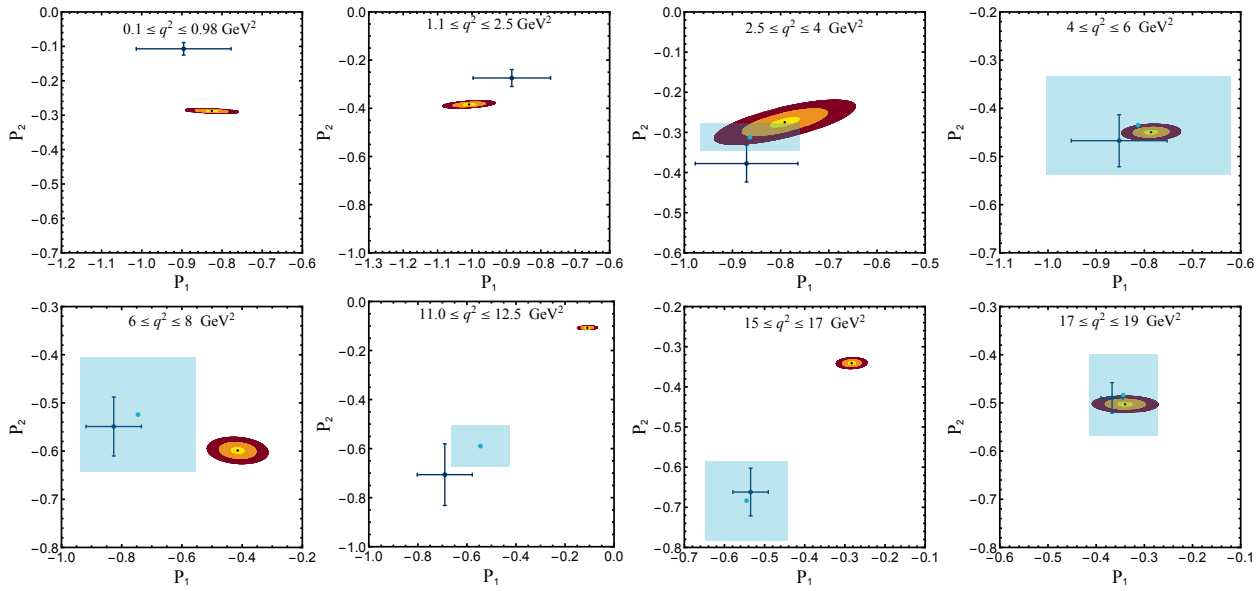

FIG. 1. (color online). The allowed region for P_1 versus P_2 plane. The innermost yellow (lightest), the middle one orange (light) and outer most red (dark) contours represent 1σ, 3σ and 5σ regions, respectively. The theoretically estimated values using Ref. [10] for $q^2 \leq 8$ GeV^2 and Ref. [14] for $q^2 \geq 11$ GeV^2 are shown as points with error bars. The light blue bands denote exact solutions for the SM observables including charmonium resonances from Ref. [17] parametrization and are shown only for the relevant q^2 bins. In most cases, there is reasonable agreement between the theoretical values and those obtained from data. However, for the ranges $0.1 \leq q^2 \leq 0.98$GeV^2, $6 \leq q^2 \leq 8$GeV^2, $11.0 \leq q^2 \leq 12.5$ GeV^2 and $15 \leq q^2 \leq 17$ GeV^2 there are significant disagreements.

where,

$$\zeta = \frac{\mathcal{F}_\perp^2 C_{10}^2}{\Gamma_f}, \tag{14}$$

$$u_\lambda^2 = \frac{2\mathcal{F}_\perp^2 r_\lambda^2}{\Gamma_f} = \frac{2}{\Gamma_f}\frac{\mathcal{F}_\perp^2}{\mathcal{F}_\lambda^2}\Big(\mathrm{Re}(\widetilde{\mathcal{G}}_\lambda) - \mathrm{Re}(\widetilde{C}_9^\lambda)\mathcal{F}_\lambda\Big)^2. \tag{15}$$

u_λ is always taken to be positive and the sign ambiguities introduced in Eqs. (11)-(13) ensure that we can make this assumption. The five observables $F_\perp$, F_L, $A_{\rm FB}$, A_5 and A_4 have been expressed above in terms of five parameters P_1, P_2, ζ, u_0 and $u_\perp$. The other three observables A_7, A_8 and A_9 have already been used to solve for the three ε_λ values which are presented in Ref. [2]. It may be noted that since $F_\parallel = 1 - F_L - F_\perp$, $u_\parallel$ is not independent and is related to the other parameters by, $u_\parallel^2 = \mathsf{P}_1^2\big(1 - \mathsf{P}_2^{-2}(u_0^2 + 2\zeta) - (u_\perp^2 + 2\zeta)\big) - 2\zeta$.

In Refs. [2, 3] a relation depending on observables including all possible effects within SM which was derived as,

$$\sqrt{4\Big(F_L + F_\parallel + \sqrt{2}\pi A_4\Big)F_\perp - \frac{16}{9}\Big(A_{\rm FB} + \sqrt{2}A_5\Big)^2} = \sqrt{4F_\parallel F_\perp - \frac{16}{9}A_{\rm FB}^2} + \sqrt{4F_L F_\perp - \frac{32}{9}A_5^2}. \tag{16}$$

This equation can be used to express any of the observables in terms of the others. A solution for A_4 [3] is

$$A_4 = \frac{8A_5 A_{\rm FB}}{9\pi F_\perp} + \frac{\sqrt{4F_\parallel F_\perp - \frac{16}{9}A_{\rm FB}^2}\sqrt{4F_L F_\perp - \frac{32}{9}A_5^2}}{2\sqrt{2}\pi F_\perp}. \tag{17}$$

Whereas, the solution for A_5 and $A_{\rm FB}$ are given by,

$$A_5 = \frac{\pi A_4 A_{\rm FB}}{2F_\parallel} \pm \frac{3\sqrt{4F_\parallel F_\perp - \frac{16}{9}A_{\rm FB}^2}\sqrt{2F_\parallel F_L - \pi^2 A_4^2}}{8F_\parallel}, \tag{18}$$

$$A_{\rm FB} = \frac{\pi A_4 A_5}{F_L} \pm \frac{3\sqrt{4F_L F_\perp - \frac{32}{9}A_5^2}\sqrt{2F_\parallel F_L - \pi^2 A_4^2}}{4\sqrt{2}F_L}. \tag{19}$$

It may noted that Eqs. (17), (18) and (19) depend only on observables and not on any theoretical parameters and thus provides an exact test of the gauge structure of SM with experimental measurements.

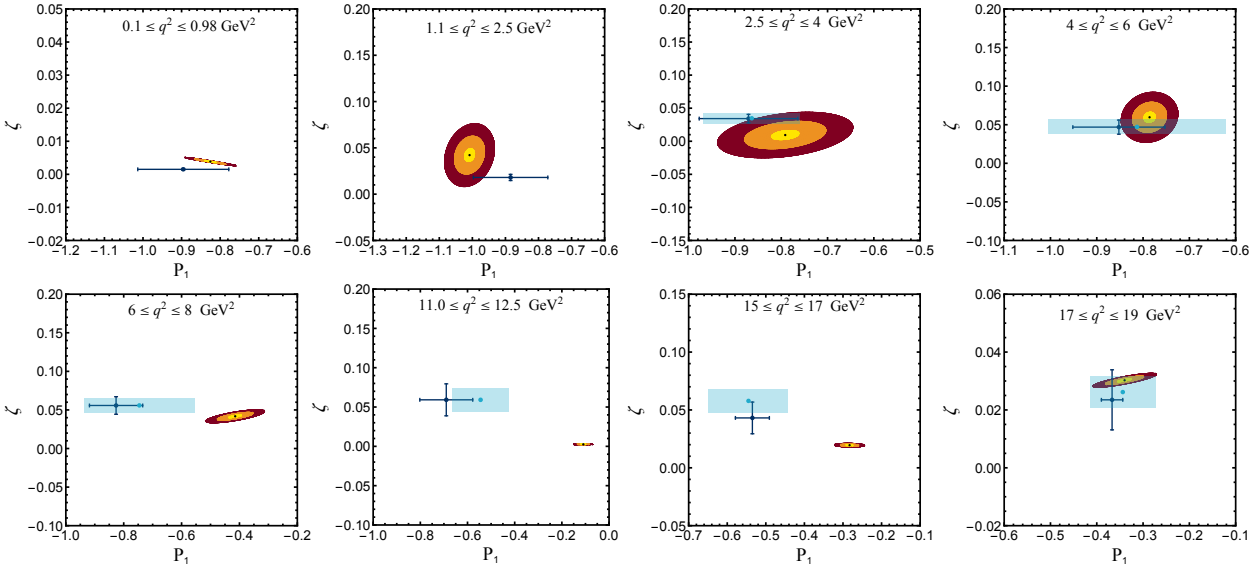

FIG. 2. (color online). The allowed region for P_1 versus ζ plane. The color code is same as Fig. 1. The theoretically estimated values from Ref. [10, 14] are shown as points with error bars. The P_1 and ζ values significantly disagree for ranges $6 \le q^2 \le 8\text{GeV}^2$, $11.0 \le q^2 \le 12.5$ GeV^2 and $15 \le q^2 \le 17$ GeV^2, similar to the values of P_1 and P_2 shown in Fig. 1.

III. NEW PHYSICS ANALYSIS

In this section we discuss the detailed numerical analysis using $3\,\text{fb}^{-1}$ of LHCb data [4]. It contains two different parts, at first we show how the experimental data can be used to extract out the form factors which are involved in this decay mode. Secondly we present the consistency of data to test the relation among observables derived relying only on the gauge structure of SM.

A. Form Factor Extraction

We demonstrate the technique to extract out the hadronic parameters by including complex contributions of the amplitudes and considering systematic uncertainty arising mainly due to bin average effect.

It is shown in Ref. [2] that ε_λ's contribute to the helicity fractions F_λ and asymmetry A_4. We refer to Appendix. A for thorough details of evaluation of the complex part of the amplitudes. Using the bin average central values of $\varepsilon_\lambda/\sqrt{\Gamma_f}$, with $\pm1\sigma$ errors from Table. III we can numerically separate out the complex contributions from experimental measured values of the observables. We calculate the central value with $\pm1\sigma$ error of the modified observables $F_\lambda^{\text{ex}\prime}$ and $A_4^{\text{ex}\prime}$ given by,

$$F_\lambda^{\text{ex}\prime} = F_\lambda^{\text{ex}} - \frac{2\varepsilon_\lambda^2}{\Gamma_f}, \tag{20}$$

$$A_4^{\text{ex}\prime} = A_4^{\text{ex}} - \frac{2\sqrt{2}\varepsilon_0\varepsilon_\parallel}{\pi\Gamma_f}, \tag{21}$$

which enter in the χ^2 definition Eq. (23) below. It enables us to take into account the complex corrections in our analysis and extract out the variables P_1, P_2, ζ, u_0 and $u_\perp$ (which only deal with the real part of amplitude) from experimental measurements of the observables accurately.

It should be noted that Eqs. (9) – (13) are valid for each q^2 point. However, experiments can provide bin integrated values of observables over a certain q^2 intervals. Thus a χ^2 fit with bin average values of the observables may lead to a biased conclusion. To avoid this issue we have added systematic uncertainties for each observables due to bin average effect with the introduction of new parameter β, where the change in each observable $\mathcal{O}$ is given by,

$$\mathcal{O} \to \mathcal{O} + \beta\,\mathcal{O}^s. \tag{22}$$

$\mathcal{O}^s$ is the maximum shift for each observables with a best fitted q^2 function to 14 bin LHCb data [4] within the concerned bin interval. The precise determination of $\mathcal{O}^s$ is described in Appendix. B. Therefore the χ^2 definition is

$$\chi^2 = \left[\left(\frac{F_\perp^{\text{ex}\prime} - F_\perp - \beta F_\perp^s}{\Delta F_\perp^{\text{ex}\prime}}\right)^2 + \left(\frac{F_L^{\text{ex}\prime} - F_L - \beta F_L^s}{\Delta F_L^{\text{ex}\prime}}\right)^2 + \left(\frac{A_4^{\text{ex}\prime} - A_4 - \beta A_4^s}{\Delta A_4^{\text{ex}\prime}}\right)^2 + \left(\frac{A_{\text{FB}}^{2\,\text{ex}} - A_{\text{FB}}^2 - \beta A_{\text{FB}}^{2s}}{2A_{\text{FB}}^{\text{ex}}\Delta A_{\text{FB}}^{\text{ex}}}\right)^2 + \left(\frac{A_5^{2\,\text{ex}} - A_5^2 - \beta A_5^{2s}}{2A_5^{\text{ex}}\Delta A_5^{\text{ex}}}\right)^2 + \beta^2\right], \tag{23}$$

where $A_{\text{FB}}^{\text{ex}}$ and A_5^{ex} indicate experimental central values of the observables A_{FB} and A_5 with $\pm1\sigma$ errors as $\Delta A_{\text{FB}}^{\text{ex}}$ and ΔA_5^{ex}, respectively. Similarly $F_\perp^{\text{ex}\prime}$, $F_L^{\text{ex}\prime}$ and

$A_4^{ex\prime}$ are the central values of the modified observables defined in Eqs. (20) and (21) and $\Delta F_\perp^{ex\prime}, \Delta F_L^{ex\prime}, \Delta A_4^{ex\prime}$ are $\pm 1\sigma$ uncertainties in it. The systematic uncertainties added for each observables are denoted as $F_\perp^s$, F_L^s, A_4^s, $A_{\rm FB}^{2s}$, A_5^{2s} and these values are quoted in Table. IV of Appendix. B. The observables $F_\perp$, F_L, A_4, $A_{\rm FB}^2$ and A_5^2 are evaluated in terms of the five parameters P_1, P_2, ζ, u_0 and $u_\perp$ using Eqs. (9) – (13). Considering the inverse of the covariance matrix the error ellipsoids are constructed for all the eight bins corresponding to the q^2 values in the range $(0.1-0.98)$ GeV^2, $(1.1-2.5)$ GeV^2, $(2.5-4.0)$ GeV^2, $(4-6)$ GeV^2, $(6-8)$ GeV^2, $(11.0-12.5)$ GeV^2, $(15-17)$ GeV^2 and $(17-19)$ GeV^2. It can be seen that β is treated as a nuisance parameter with values 0 ± 1. The χ^2 function is minimized w.r.t six parameters P_1, P_2, ζ, u_0, $u_\perp$ and β and the contours shown in Fig. 1 and Fig. 2 are the allowed regions in the corresponding planes. The minimum values of the χ^2 function for first to eighth bins are 6.9×10^{-9}, 3.4×10^{-10}, 0.055, 8.6×10^{-30}, 1.094, 0.538, 0.218 and 0.044, respectively. The best fitted values with $\pm1\sigma$ errors of the parameter β for all eight bins are $7.4\times10^{-5}\pm0.015$, $1.6\times10^{-5}\pm0.020$, 0.153 ± 0.011, $1.0\times10^{-17}\pm0.005$, 0.736 ± 0.020, 0.251 ± 0.003, 0.261 ± 0.001 and 0.161 ± 0.012, respectively.

The contours corresponding to 1σ, 3σ and 5σ permitted regions for P_1 versus P_2 plane are presented in Fig. 1. These contours are compared with the estimated values of P_1 and P_2 using Ref. [10] for $q^2\le 8$ GeV^2 and Ref. [14] for $q^2\ge 11$ GeV^2. The center black point denotes the best fit point by minimizing the chi-square function defined in Eq. (23). In most cases reasonable agreement is found between theoretical values of P_1 and P_2 and their values obtained from data. However, there are some significant disagreements. The values of form factor ratio P_2 differ by 9σ in the $0.1\le q^2\le 0.98$ GeV^2 bin. It may be noted that this region in q^2 is highly affected by finite lepton mass and hence the large discrepancy may not accurately reflect the significance due to the unaccounted lepton mass correction systematics. Significant deviations are also found for the three bins $6\le q^2\le 8$ GeV^2, $11.0\le q^2\le 12.5$ GeV^2 and $15\le q^2\le 17$ GeV^2 where P_1 (P_2) differ by 4.2σ (0.8σ), 5.2σ (4.8σ) and 5.5σ (5.3σ), respectively. The light blue bands denote exact solutions for the SM observables including charmonium resonances from Ref. [17] parametrization and are shown only for the relevant q^2 bins. The detailed analysis of resonance effect will be discussed later in this section.

In Fig. 2 contours similar to Fig. 1, but corresponding to P_1 versus ζ permitted regions are presented for 1σ, 3σ and 5σ confidence level regions. These contours are similarly compared with the estimated values of P_1 and ζ using Refs. [10, 14] and assuming the theoretical estimate of C_{10} [15]. Data shows consistency with theoretical values of P_1 and ζ in most cases except for the two bins $11.0\le q^2\le 12.5$ GeV^2 and $15\le q^2\le 17$ GeV^2 where ζ disagrees by 2.8σ and 1.7σ respectively. The best fit value of ζ with $\pm1\sigma$ error obtained from the fit can be used to calculate the form factor $\mathcal{F}_\perp$ using Eq. (14).

q^2 range in GeV^2	$V(q^2)$	$A_1(q^2)$	$A_{12}(q^2)$
$0.1\le q^2\le 0.98$	0.677 ± 0.092 (3.05σ)	0.570 ± 0.077 (3.40σ)	0.246 ± 0.034 (0.88σ)
$1.1\le q^2\le 2.5$	0.625 ± 0.071 (2.78σ)	0.409 ± 0.046 (2.00σ)	0.326 ± 0.047 (0.69σ)
$2.5\le q^2\le 4.0$	0.230 ± 0.150 (1.36σ)	0.180 ± 0.118 (1.09σ)	0.214 ± 0.149 (0.81σ)
$4.0\le q^2\le 6.0$	0.552 ± 0.043 (1.07σ)	0.400 ± 0.032 (1.69σ)	0.359 ± 0.041 (1.09σ)
$6.0\le q^2\le 8.0$	0.485 ± 0.045 (1.27σ)	0.598 ± 0.073 (3.18σ)	0.252 ± 0.025 (1.78σ)
$11.0\le q^2\le 12.5$	0.166 ± 0.018 (5.64σ)	0.560 ± 0.065 (1.76σ)	0.450 ± 0.054 (1.81σ)
$15.0\le q^2\le 17.0$	0.828 ± 0.120 (2.79σ)	0.649 ± 0.098 (1.38σ)	0.496 ± 0.074 (1.51σ)
$17.0\le q^2\le 19.0$	1.813 ± 0.436 (0.78σ)	0.698 ± 0.171 (0.80σ)	0.461 ± 0.112 (0.91σ)

TABLE I. The form factor values obtained from fit to $3\,\text{fb}^{-1}$ of LHCb data [4]. Round brackets indicate the standard deviation between fitted values and theoretical estimates [10, 14]. Significant discrepancies are found for V and A_1 in several q^2 region.

Finally the form factor V can be evaluated using Eq. (4a) and the value of $\mathcal{F}_\perp$ obtained. Since the recent $3\,\text{fb}^{-1}$ of LHCb result [4] does not provide branching fraction measurement for the entire q^2 region we assume the theoretical values of Γ_f [10, 14] in addition to C_{10} [15]. The form factors $\mathcal{F}_\parallel$ and $\mathcal{F}_0$ can then be determined from the fits to P_1 and P_2 respectively, using Eq. (8). Thus the conventional form factors A_1 and A_{12} can easily be estimated with the relation given in Eqs. (4b) and (4c). In Table. I we list the best fit values with the 1σ uncertainties for the three form factors $V(q^2)$, $A_1(q^2)$ and $A_{12}(q^2)$ for all the eight q^2 intervals. We also present the standard deviation of the fit compared to the theoretical estimate from Refs. [10, 14]. While sizable discrepancy is seen for all the form factors especially in the regions $q^2<2.5$ GeV^2 and $q^2>6$ GeV^2. It is interesting to note the very significant discrepancy is observed in the values of form factors V and A_1 in bins $0.1\le q^2\le 0.98$ GeV^2, $1.1\le q^2\le 2.5$ GeV^2, $6\le q^2\le 8$ GeV^2, $11.0\le q^2\le 12.5$ GeV^2 and $15\le q^2\le 17$ GeV^2. The lattice estimate of the form factors currently does not include finite K^* width. This implies, that the significance of the deviations can be lower if one includes the unaccounted systematics due to the finite K^* width. We point out that previous attempts to incorporate resonance contributions in theory has been done by parametrically taking its effect in the Wilson coefficient C_9 [16, 17]. However the accuracy of the form of resonance parametrization does not alter our determination of form factors since, our analysis is independent of $\widetilde{C}_9^\lambda$ estimates. $\widetilde{C}_9^\lambda$ contributes only to u_λ's and *the ratios of form factors* P_1 *and* P_2 *do not get*

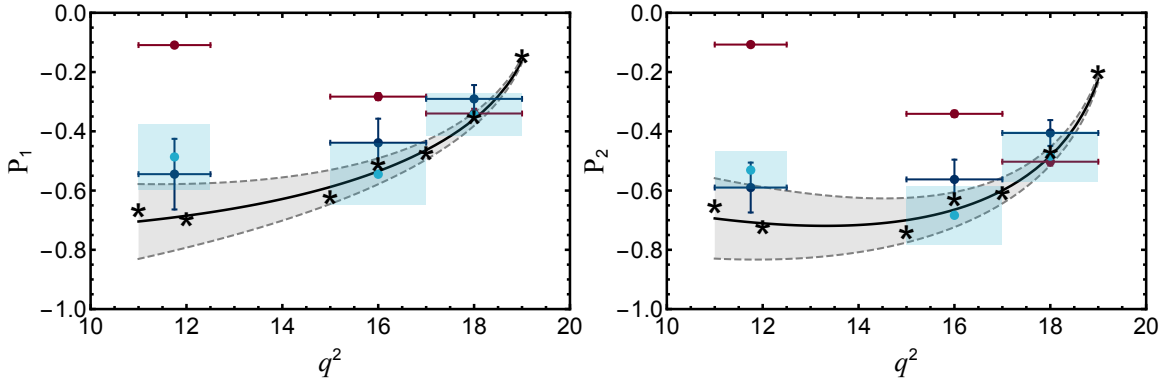

FIG. 3. (color online) Illustrative plots for bin average and resonance effects in the solutions for P_1 (left panel) and P_2 (right panel). The SM observables are assumed from lattice form factors [14]. The black 'stars' denote the solutions obtained at seven different points in q^2 for the corresponding parameters in each plot. The black central curve with gray band is the form factor estimate (mean with $\pm 1\sigma$ error) of P_1 and P_2. The blue error bars are the solutions for P_1 and P_2 using the bin average values of SM observables whereas the light blue bands denote the solutions considering resonances in observables from Ref. [17] parametrization. The red error bars denote the solutions obtained using data (as highlighted in contours is Fig. 1). Including the resonances with the parametrization used in Ref. [17], the solutions for P_1 and P_2 are unaltered and superimpose with the 'stars' completely. (see text for details)

affected by resonances. This is easily seen if we consider a situation where NP is absent and all the parameters for resonances (strength, phase etc.) are known, the observables calculated using Eqs. (9)–(13) should agree with the experimental measured observables. Thus the consistent set of Eqs. (9)–(13) must provide the same set of parameters that we would have started with, as best fit solutions. In the absence of NP the measured observables should result in the solutions for parameters matching with SM values. Since P_1 and P_2 are unaffected by resonances their best fit solutions also remain unaffected by it. Our best fit values of P_1 and P_2 differ from the SM estimates and this discrepancy cannot be accounted for by resonances.

To establish the above arguments we further undertake an extensive study illustrated in Fig. 3. We choose the region $q^2 > 11\,\text{GeV}^2$ as resonance effects can be dominant here and assume SM form factor values of the observables from lattice calculations [14]. The solutions for P_1 and P_2 are obtained using Eqs. (9)–(13) for seven different q^2 points; $11\,\text{GeV}^2$, $12\,\text{GeV}^2$, $15\,\text{GeV}^2$, $16\,\text{GeV}^2$, $17\,\text{GeV}^2$, $18\,\text{GeV}^2$ and $19\,\text{GeV}^2$. The observables $F_\perp$, F_L, A_4, A_{FB}^2 and A_5^2 are SM estimates calculated using lattice form factors. These seven solutions of P_1 and P_2 are denoted by 'star' symbols in the corresponding plots. The black central line with gray band is the form factor estimate (mean with $\pm 1\sigma$ error) of P_1 and P_2. It can be seen that the set of Eqs. (9)–(13) are completely consistent with SM structure and produces expected solutions. In case the solutions were completely analytically obtained, the 'stars' should sit on the black curves. However the solutions for hadronic parameters are very complicated and has been evaluated numerically, resulting in small shifts that are visible. The blue error bars are the solutions for P_1 and P_2 using the bin average values of SM observables. It can be seen that as the Eqs. (9)–(13) are valid at each q^2 point, bin averaging has induced some shifts in the solutions. However the results are in agreement within $\pm 1\sigma$ confidence level region. To illustrate the effect of resonances we have considered the parametrization from Ref. [17]. The charmonium bound states $J/\psi(1S)$, $\psi(2S)$, $\psi(3770)$, $\psi(4040)$, $\psi(4160)$ and $\psi(4415)$ are included in the mentioned five observables. Interestingly, the change in the value of observables including the resonances affected the solutions for ζ, $u_\perp$ and $u_\parallel$, however, solutions to P_1 and P_2 remained unaltered (upto second decimal place), hence, the solutions completely superimpose with the 'stars' obtained without resonance contributions. We have also investigated the effect of resonances in the bin average where the observables are evaluated with lattice form factors including the above mentioned resonances and the solutions to P_1 and P_2 are shown in light blue bands for the three q^2 bins $11.0 \le q^2 \le 12.5$ GeV^2, $15 \le q^2 \le 17$ GeV^2 and $17 \le q^2 \le 19$ GeV^2. In this case the results with and without resonances do not completely superimpose however are quite consistent within $\pm 1\sigma$ error bars. These solutions are also shown in Fig. 1 and 2, in same light blue bands, for the relevant bins where resonance effect may in principle be significant. The red error bars are the solutions for P_1 and P_2 obtained from data (as discussed and highlighted in contours is Fig. 1) that have been shown here again for convenience. We reiterate that effect of resonances in P_1, P_2 solutions is independent of the parametrization choice as the solutions do not depend on Wilson coefficient $\widetilde{C}_9^\lambda$ and our conclusions derived for P_1 and P_2 parameters are unaffected by resonance effect. It is justified that bin average can induce some errors in the solutions. However, we have allowed a shift in the

observable values (in Eq. 23 and Table. IV) of more than the 1σ error for each observable which hopefully is sufficient to compensate such effects.

It is important to note that in our analysis no hadronic estimates are used to solve for the five parameters from exactly five measurements. Whereas, in other approaches, when considering the same $B \to K^* \ell\ell$ mode all six form factors, Wilson coefficients and non factorisable corrections based on conservative estimations are needed. We compare P_1 and P_2 obtained from experimental data alone, with the three form factor V, A_1 and A_{12} to which they are related as theoretical inputs. The form-factors T_1, T_2 and T_{23} are not used in this comparison. Thus, our comparisons are different in nature and have reduced uncertainties, in terms of number of theoretical estimates. This may result in higher significance level of deviation observed here.

The large q^2 region where the K^* has low-recoil energy has also been studied [18, 19] in a modified heavy quark effective theory framework which is a model independent approach. In this limit the number of independent hadronic form factors reduces to only three and one finds [3] that $r_0 = r_\parallel = r_\perp$ or equivalently $u_0 = u_\parallel = u_\perp$ must hold as long as non-factorizable charm loop contributions are negligible. We find that this relation does not hold for either of the bins $15 \le q^2 \le 17$ GeV^2 or $17 \le q^2 \le 19$ GeV^2. The values of u_0, $u_\parallel$ and $u_\perp$ obtained from the fit with $\pm 1\sigma$ errors are listed in Table II. We note that u_λ's receive problematic resonance contribution coming from $\widetilde{C}_9^\lambda$. To address this issue we have introduced more sytematics in measured observable than the one arising only from bin average effect. We have checked our analysis by doubling the systematics of the observables given in Table. IV of Appendix. B for the q^2 range $11 \le q^2 \le 12.5$ GeV^2 and $15 \le q^2 \le 17$ GeV^2 and our results are stable with it. The actual significance of the deviations observed here can be obtained with the detailed study of resonance systematics which is a subject of an independent paper. However the significance level is evaluated by conservatively adding systematics varying between 10% – 100% in the observables. The large discrepancies observed are equally hard to explain solely due to non-factorizable charm loop corrections and may be additional evidence of physics beyond the SM.

q^2 range in GeV^2	u_0	$u_\parallel$	$u_\perp$
$15 \le q^2 \le 17$	0.000 ± 0.016	0.013 ± 0.153	0.367 ± 0.025
$17 \le q^2 \le 19$	0.166 ± 0.014	0.000 ± 4.579	0.260 ± 0.048
$15 \le q^2 \le 19$	0.120 ± 0.007	0.004 ± 0.441	0.244 ± 0.026

TABLE II. The values of u_0, $u_\parallel$ and $u_\perp$ obtained from fit to $3\,\text{fb}^{-1}$ of LHCb data [4]. In large q^2 region [18, 19] the equality $u_0 = u_\parallel = u_\perp$ is expected to hold if non-factorizable charm loop contributions are negligible. The errors in the value of $u_\parallel$ for the larger q^2 bin is unexpectedly large to draw any conclusions. Significant discrepancies which are too large to be solely due to non-factorizable charm loop corrections are observed between the values of $u_\perp$ and u_0 in both bins.

B. Testing relation between observables

The relation between the observables for asymmetries A_4, A_5 and $A_{\rm FB}$ given in Eqs. (17) – (19) can also be tested using LHCb data [4]. In Fig. 4, top left panel, we compare theoretically calculated $A_{\rm FB}$ mean values and $\pm 1\sigma$ errors (in yellow bands) with experimental measurements (red error bars) for the respective q^2 bins. All observables in the r.h.s of Eq. (19) ('relation') are assumed to be Gaussian distributions in data and the predictions for $A_{\rm FB}$ in yellow bands are obtained using the expression of the 'relation'. A very good agreement is evident for most q^2 regions, however, for the ranges $11.0 \le q^2 \le 12.5$ GeV^2 and $15 \le q^2 \le 17$ GeV^2 a deviation of 2.1σ and 1.8σ is observed. Similarly 'relation' for A_4 in Eq. (17) results in a very good agreement except for showing a discrepancy of 2.3σ only in the $0.1 \le q^2 \le 0.98$ GeV^2 bin, in right top panel of Fig. 4. The disagreement in the value of $A_{\rm FB}$ and A_4 in some q^2 bins indicates that there is no set of form factors and Wilson coefficients which can explain $A_{\rm FB}$ and A_4 completely. Observables A_5 or equivalently P_5' [20] are found to be in complete agreement i.e. within about $\pm 1\sigma$ deviation for all q^2 bins as shown in the two lower panels of Fig. 4. The solutions for A_5 and $A_{\rm FB}$ have ambiguities. We chose the ambiguity for which the chi-squared deviations are the least. Our conclusions have no bearing on and do not rule out the observation made by LHCb in observable P_5' in Refs. [4, 9]. The predictions of observable P_5' derived from the relation is a signal of consistency of LHCb results. We note that the relation remains valid except in the presence of NP operators that result in modified new angular distribution. Hence we do not expect to see the discrepancy observed by LHCb [9] if right-handed currents or extra vector current such as Z' contributes to the decay. The discrepancy observed by LHCb depends on the comparison with model based calculation of form factors. Whereas, the predictions of these asymmetries made in this paper, are independent of any form factor values and depend purely on the gauge structure of SM. If the model dependent calculations of form factors are correct, signal of new physics may well be indicated in the bins suggested by Ref. [9]. We find that LHCb data indicates yet another independent discrepancy.

IV. CONCLUSION

In conclusion, we have used the $3\,\text{fb}^{-1}$ of LHCb data to determine some hadronic parameters governing the decay $B \to K^* \ell^+ \ell^-$ assuming contributions from SM alone. We obtain the values of the form factors $V(q^2)$, $A_1(q^2)$ and $A_{12}(q^2)$ that are used to describe the matrix element $\langle K^* | \bar{s} \gamma^\mu P_L b | B \rangle$ directly from data. Very significant deviations are seen for the form factors V and A_1 especially in the regions $q^2 < 2.5$ GeV^2 and $q^2 > 6$ GeV^2. We point out that the presence of resonances in data can induce more systematic uncertainties in the fits. How-

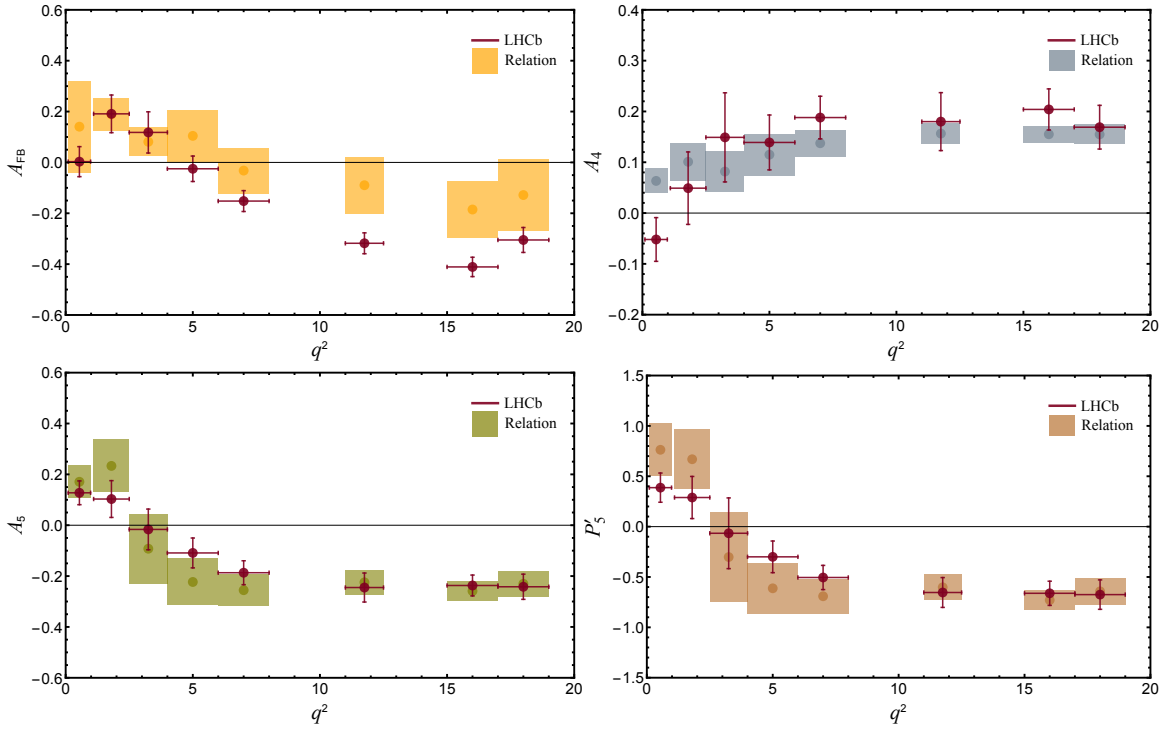

FIG. 4. (color online) The mean values and $\pm 1\sigma$ uncertainty bands for asymmetries $A_{\rm FB}$, A_4, A_5 and P_5' calculated using Eqs. (17) – (19) are shown in yellow, gray, green and brown bands, respectively. The error bars in red (dark) correspond to the LHCb measured [4] central values and errors for each observable for the respective q^2 bins. The predictions for the asymmetries are obtained using the relations among observables which are independent of any hadronic parameters and depend on experimental measurements of the other observables remaining in the corresponding relations. Sizable discrepancies are shown for $A_{\rm FB}$ in $11.0 \leq q^2 \leq 12.5$ GeV^2 and $15 \leq q^2 \leq 17$ GeV^2 bins and for A_4 in the range $0.1 \leq q^2 \leq 0.98$ GeV^2. We note that the relations (Eqs. (17) – (19)) remain valid except in the presence of NP operators that result in modified angular distribution. Hence the presence of right-handed currents and any extra vector current such as Z' the relations will remain valid.

ever in the view of absence of such a existence of resonances in $B \to K^* \ell^+ \ell^-$ data, we emphasize that the significant deviations observed in the form factor values can not be completely explained by resonances and non-factorizable contributions. We would like to point out that there exist major differences between the global fit approaches [6] to study the anomalies in $b \to s$ transitions and the approach adopted in our work. Our work relies only on $B \to K^* \ell\ell$ decay mode, whereas, global fit techniques incorporate various decay modes and hence either use LCSR, Lattice based estimates of form factors or treat form-factors as parameters in the fit procedure. The number of inputs and fitted parameters differ making a number by number comparison of the different approaches difficult. Furthermore due to the absence of accurate estimates of non factorisable corrections, the global fit techniques rely on some conservative estimations of these corrections. However, the formalism we have developed parametrizes such corrections and the conclusions drawn here are independent of non factorisable estimates. These are perhaps the reasons why we find larger significance. However, qualitatively we don't see a significant disagreement with the other approaches as we do observe $\sim 3\sigma$ discrepancy in $\mathsf{P}_1 - \mathsf{P}_2$ plane in q^2 region $[6-8]$GeV^2 where observable P_5' also deviates by 2.7σ from its SM prediction.

Further, a relation between form factors expected to hold in the large q^2 region as long as non-factorizable charm loop contributions are negligible, seems to fail. Finally, the relation between observables also indicates some deviations in the same regions where the form factors were found to disagree. The forward-backward asymmetry $A_{\rm FB}$ deviates in the $q^2 > 11$ GeV^2 region, where as A_4 differs in the region $q^2 \leq 0.98$ GeV^2. As the systematic error arises from the experimental measurements of observables in terms of binned dilepton invariant mass are accounted, the magnitude of discrepancies observed would be hard to accommodate either as systematics from long distance resonance contributions or possible corrections to theoretical estimates. All these features can be understood if there are other unaccounted for operators contributing to the decay mode. In view of this, we speculate that these deviations are likely to be a signature of physics beyond SM.

ACKNOWLEDGMENTS

We are indebted to Tom Browder and thank him for several suggestions and discussions. We also thank J. Martin Camalich, Hai-Yang Cheng, N. G Deshpande, Jim Libby and Arjun Menon for discussions. R.S. thanks Hai-Yang Cheng and Institute of Physics, Academia Sinica, Taipei, Taiwan for hospitality during final stages of manuscript preparation.

Appendix A: Complex contribution ε_λ estimates from data

In Ref. [2] it was shown that the complex contributions ε_λ to the amplitude of the decay mode $B \to K^* \ell^+ \ell^-$, can be taken into consideration. ε_λ can be solved in terms of iterative solutions proportional to the observables A_7, A_8, A_9 and a form factor ratio P_1. The expressions for all the three ε_λ's are shown in Eqs. (76)–(78) of Ref. [2]. They are reproduced here for convenience.

$$\varepsilon_\perp = \frac{\sqrt{2}\pi\Gamma_f}{(r_0 - r_\parallel)\mathcal{F}_\perp}\left[\frac{A_9\mathsf{P}_1}{3\sqrt{2}} + \frac{A_8\mathsf{P}_2}{4} - \frac{A_7\mathsf{P}_1\mathsf{P}_2 r_\perp}{3\pi C_{10}}\right], \quad \text{(A1)}$$

$$\varepsilon_\parallel = \frac{\sqrt{2}\pi\Gamma_f}{(r_0 - r_\parallel)\mathcal{F}_\perp}\left[\frac{A_9 r_0}{3\sqrt{2}r_\perp} + \frac{A_8\mathsf{P}_2 r_\parallel}{4\mathsf{P}_1 r_\perp} - \frac{A_7\mathsf{P}_2 r_\parallel}{3\pi C_{10}}\right], \quad \text{(A2)}$$

$$\varepsilon_0 = \frac{\sqrt{2}\pi\Gamma_f}{(r_0 - r_\parallel)\mathcal{F}_\perp}\left[\frac{A_9\mathsf{P}_1 r_0}{3\sqrt{2}\mathsf{P}_2 r_\perp} + \frac{A_8 r_\parallel}{4r_\perp} - \frac{A_7\mathsf{P}_1 r_0}{3\pi C_{10}}\right]. \quad \text{(A3)}$$

A point to be noted as explained in detail in Ref. [2], is that the $(\varepsilon_\lambda/\Gamma_f^{1/2})$'s are completely expressed in terms of observables and the form factor ratio P_1. However, these solutions are essentially iterative, since the r_λ's and C_{10} are derived in terms of the primed observables that depend on ε_λ. If $(\varepsilon_\lambda/\Gamma_f^{1/2})$ are small as should be expected, accurate solutions for them can be found with a few iterations. In Ref. [2] the variation of ε_λ with P_1 was studied for $1\,\text{fb}^{-1}$ LHC data and it was found that the solutions are not sensitive to the value of P_1.

We generate a set of events for every bin, with each event consisting of randomly chosen values drawn from Gaussian distributions generated for each of the observables F_L, $F_\perp$, A_4, A_5, $A_{\rm FB}$, A_7, A_8 and A_9. The distributions are generated using experimental results from Ref. [4], with the experimentally measured value as mean and the uncertainty as standard deviation.

ε_λ are solved iteratively for every set of observables. We find converged iterative solutions for $\varepsilon_\lambda/\sqrt{\Gamma_f}$ for each set of observables with the histograms shown in Fig. 5. The red (dark), light brown (lightest) and green histograms denote the solutions for $\varepsilon_\perp/\sqrt{\Gamma_f}$, $\varepsilon_\parallel/\sqrt{\Gamma_f}$ and $\varepsilon_0/\sqrt{\Gamma_f}$ respectively for all the eight bins with q^2 range $(0.1 - 0.98)$ GeV^2, $(1.1 - 2.5)$ GeV^2, $(2.5 - 4.0)$ GeV^2, $(4 - 6)$ GeV^2, $(6 - 8)$ GeV^2, $(11.0 - 12.5)$ GeV^2, $(15 - 17)$ GeV^2 and $(17 - 19)$ GeV^2.

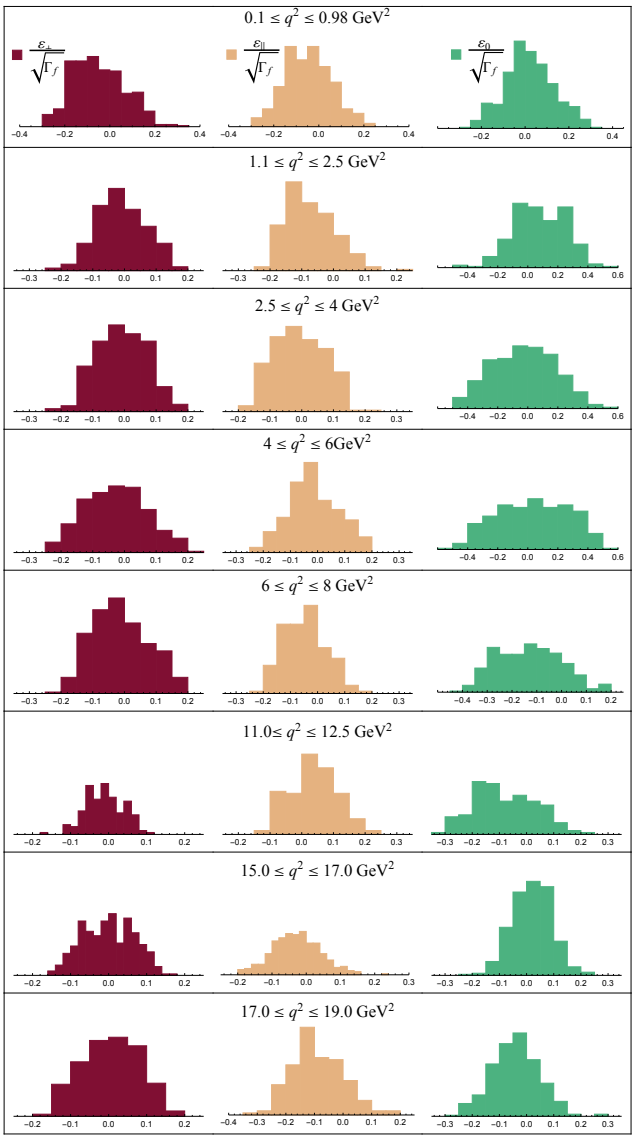

FIG. 5. (color online) The solutions for $\varepsilon_\perp/\sqrt{\Gamma_f}$, $\varepsilon_\parallel/\sqrt{\Gamma_f}$ and $\varepsilon_0/\sqrt{\Gamma_f}$ using distributions for first through eighth q^2 bins are depicted in red (dark), light brown (lightest) and green respectively. All the $\varepsilon_\lambda/\sqrt{\Gamma_f}$'s are consistent with zero.

We have also quoted the mean and $\pm 1\sigma$ errors for each $\varepsilon_\lambda/\sqrt{\Gamma_f}$ in Table. III calculated from the distributions shown in Fig. 5. It can be easily seen that all the mean values of $\varepsilon_\lambda/\sqrt{\Gamma_f}$ are consistent with zero. From Eqs. (37)–(40) of Ref. [2], the contributions from imaginary part of the amplitude to the observables F_L, $F_\parallel$, $F_\perp$ and A_4 are quadratic in the corresponding $\varepsilon_\lambda/\sqrt{\Gamma_f}$ and thus are negligible.

q^2 in GeV^2	$\varepsilon_\perp/\sqrt{\Gamma_f}$	$\varepsilon_\parallel/\sqrt{\Gamma_f}$	$\varepsilon_0/\sqrt{\Gamma_f}$
$0.1 \le q^2 \le 0.98$	-0.048 ± 0.116	-0.047 ± 0.103	0.020 ± 0.111
$1.1 \le q^2 \le 2.5$	-0.010 ± 0.078	-0.010 ± 0.078	0.078 ± 0.172
$2.5 \le q^2 \le 4.0$	-0.009 ± 0.079	-0.008 ± 0.080	-0.025 ± 0.212
$4.0 \le q^2 \le 6.0$	-0.026 ± 0.097	0.014 ± 0.093	0.032 ± 0.234
$6.0 \le q^2 \le 8.0$	-0.011 ± 0.088	-0.046 ± 0.078	-0.132 ± 0.129
$11.0 \le q^2 \le 12.5$	-0.011 ± 0.050	0.038 ± 0.074	-0.078 ± 0.114
$15.0 \le q^2 \le 17.0$	-0.000 ± 0.067	-0.027 ± 0.071	0.020 ± 0.072
$17.0 \le q^2 \le 19.0$	0.006 ± 0.076	-0.090 ± 0.090	-0.040 ± 0.088

TABLE III. The $\varepsilon_\lambda/\sqrt{\Gamma_f}$ mean values with $\pm 1\sigma$ errors from Fig. 5

Appendix B: Systematic uncertainty evaluation

q^2 range in GeV^2	$F_\perp^s$	F_L^s	A_4^s	$A_{\rm FB}^{2s}$	A_5^{2s}
$0.1 \le q^2 \le 0.98$	0.014	0.230	0.088	0.002	0.016
$1.1 \le q^2 \le 2.5$	0.223	0.151	0.036	0.034	0.010
$2.5 \le q^2 \le 4.0$	0.164	0.223	0.064	0.013	0.004
$4.0 \le q^2 \le 6.0$	0.069	0.138	0.021	0.002	0.008
$6.0 \le q^2 \le 8.0$	0.132	0.165	0.028	0.020	0.019
$11.0 \le q^2 \le 12.5$	0.029	0.063	0.006	0.051	0.023
$15.0 \le q^2 \le 17.0$	0.019	0.048	0.027	0.036	0.023
$17.0 \le q^2 \le 19.0$	0.109	0.020	0.039	0.077	0.053

TABLE IV. The systematic uncertainties for each observables $F_\perp$, F_L, A_4, $A_{\rm FB}^2$ and A_5^2 are shown. The values denote magnitude of maximum deviation of the bin average central value with the fitted q^2 polynomial within every q^2 bin.

We discuss the evaluation of systematic uncertainties arising mainly due to bin average effect of observables. As written in Eq. (22), the shift $\mathcal{O}^s$ in each observable is calculated for each q^2 bin, by considering the maximum deviation of the bin average value of the observable $\mathcal{O}$ from a fitted q^2 polynomial of entire range. It is highlighted in Fig. 6 where red error bars are LHCb measurements and gray curves represent best fitted polynomial in q^2 for 14 bin LHCb data. We use 14 bin measurement (based on the method of moments [13]) from LHCb to fit the polynomial in q^2, rather than the 8 bin data set as it provides more information to determine the shape of the polynomial for entire q^2 region. The black dashed line denotes the maximum deviation of bin average central value of the observable with the q^2 function for the region $6 \le q^2 \le 8$ GeV^2 and $\mathcal{O}^s$ is the length of the line for observable $\mathcal{O}$. Similar technique is applied for other q^2 bins also and the values of systematic errors are given in Table. IV for all observables.

It should be noted that as discussed in Sec. III finite lepton mass can affect the analysis in the first two q^2 region namely $q^2 \le 2.5$ GeV^2 and in the absence of a measurement of asymmetries A_{10} and A_{11} [2] we have to rely on some hadronic estimates. This in principle may cause more uncertainties and we took a conservative approach by considering two times the $\mathcal{O}^s$ values for all observables given in Table. IV for the two bins $0.1 \le q^2 \le 0.98$ GeV^2 and $1.1 \le q^2 \le 2.5$ GeV^2.

We emphasize that resonances in our analysis will only affect the fitted function in q^2, which in turn will induce more systematic uncertainties to the observables. We have checked the χ^2 fit (in Sub-sec. III A) by increasing the systematic uncertainties two times of the values given in Table. IV for the regions $11 \le q^2 \le 12.5$ GeV^2 and $15 \le q^2 \le 17$ GeV^2 and our results are stable with it. However a detailed study of resonance systematics on this decay mode is currently going on and will be a subject of an independent paper itself.

[1] F. Kruger, L. M. Sehgal, N. Sinha, R. Sinha, Phys. Rev. **D61**, 114028 (2000). [hep-ph/9907386].

[2] R. Mandal, R. Sinha and D. Das, Phys. Rev. D **90**, no. 9, 096006 (2014). [arXiv:1409.3088 [hep-ph]].

[3] D. Das and R. Sinha, Phys. Rev. D **86** (2012) 056006. [arXiv:1205.1438 [hep-ph]];

[4] R. Aaij *et al.* [LHCb Collaboration], JHEP **1602**, 104 (2016), [arXiv:1512.04442 [hep-ex]].

[5] F. Kruger and J. Matias, Phys. Rev. D **71**, 094009 (2005) [hep-ph/0502060], T. Hurth and F. Mahmoudi, JHEP **1404**, 097 (2014) [arXiv:1312.5267 [hep-ph]], S. Descotes-Genon, J. Matias and J. Virto, Phys. Rev. D **88**, 074002 (2013) [arXiv:1307.5683 [hep-ph]], W. Altmannshofer and D. M. Straub, Eur. Phys. J. C **73**, 2646 (2013) [arXiv:1308.1501 [hep-ph]], S. Jäger and J. Martin Camalich, JHEP **1305**, 043 (2013) [arXiv:1212.2263 [hep-ph]], J. Lyon and R. Zwicky, arXiv:1406.0566 [hep-ph], and references therein.

[6] S. Descotes-Genon, L. Hofer, J. Matias and J. Virto, JHEP **1606**, 092 (2016) [arXiv:1510.04239 [hep-ph]]; M. Ciuchini, M. Fedele, E. Franco, S. Mishima, A. Paul, L. Silvestrini and M. Valli, JHEP **1606**, 116 (2016) [arXiv:1512.07157 [hep-ph]]

[7] C. Hambrock and G. Hiller, Phys. Rev. Lett. **109**, 091802 (2012). [arXiv:1204.4444 [hep-ph]].

[8] R. Aaij *et al.* [LHCb Collaboration], Phys. Rev. Lett. **108**, 181806 (2012); arXiv:1112.3515v3 [hep-ex]; R. Aaij *et al.* [LHCb Collaboration], JHEP **1308**, 131 (2013); [arXiv:1304.6325v2 [hep-ex]];

[9] R. Aaij *et al.* [LHCb Collaboration], Phys. Rev. Lett. **111**, 191801 (2013) [arXiv:1308.1707 [hep-ex]].

[10] A. Bharucha, D. M. Straub and R. Zwicky, JHEP **1608**, 098 (2016) [arXiv:1503.05534 [hep-ph]].

[11] S. Descotes-Genon, L. Hofer, J. Matias and J. Virto, JHEP **1412** (2014) 125. [arXiv:1407.8526 [hep-ph]].

[12] A. Khodjamirian, T. Mannel, A. A. Pivovarov and Y.-M. Wang, JHEP **1009**, 089 (2010), [arXiv:1312.6480 [hep-ph]].

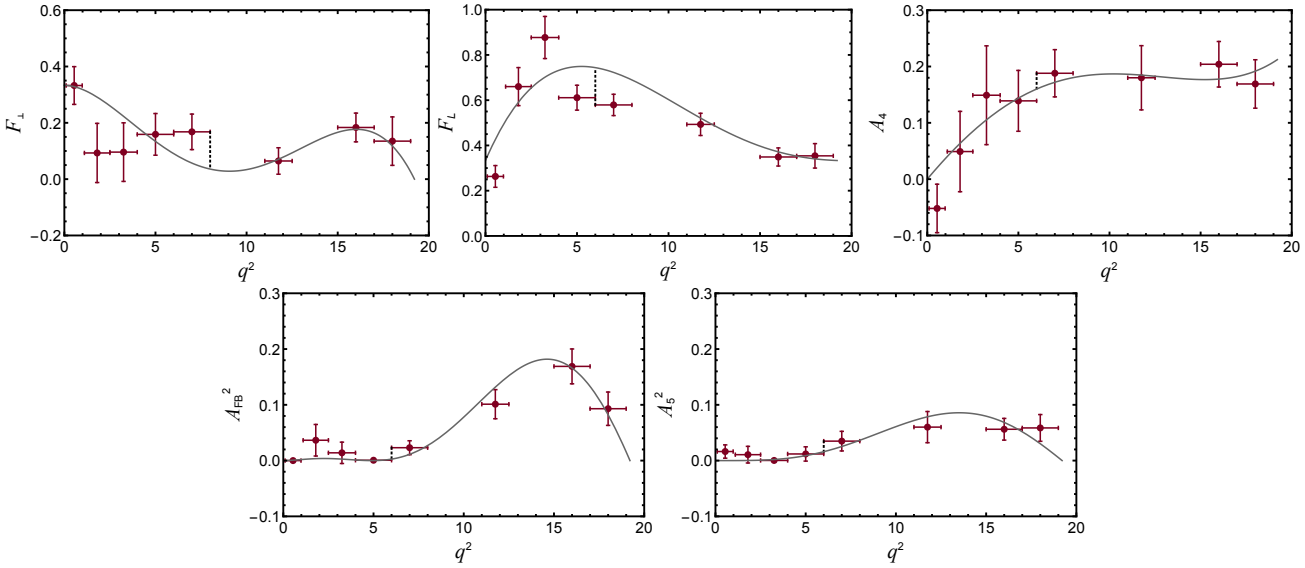

FIG. 6. (color online). The procedure to calculate systematic errors are shown for observables $F_\perp$, F_L, A_4, $A^2_{\rm FB}$ and A^2_5, respectively. The red error bars are LHCb measurements and gray curves represent best fitted polynomial in q^2 for 14 bin LHCb data [4]. The black dashed lines denote the maximum deviation of bin average central value of the observables with the q^2 function for bin $6 \leq q^2 \leq 8$ GeV^2. The length of these black lines are denoted by $F^s_\perp$, F^s_L, A^s_4, $A^{2s}_{\rm FB}$ and A^{2s}_5, respectively. Similar lines can be drawn for other q^2 bins also and the values of systematic errors are given in Table. IV for all observables.

M. Beneke and T. Feldmann, Nucl. Phys. B **592** (2001)3;

[13] F. Beaujean, M. Chrzaszcz, N. Serra and D. van Dyk, Phys. Rev. D **91**, 114012 (2015) [arXiv:1503.04100 [hep-ex]].

[14] R. R. Horgan, Z. Liu, S. Meinel and M. Wingate, Phys. Rev. Lett. **112**, 212003 (2014); [arXiv:1310.3887 [hep-ph]]; R. R. Horgan, Z. Liu, S. Meinel and M. Wingate, arXiv:1501.00367 [hep-lat].

[15] W. Altmannshofer, P. Ball, A. Bharucha *et al.*, JHEP **0901**, 019 (2009). [arXiv:0811.1214 [hep-ph]].

[16] N. G. Deshpande, J. Trampetic and K. Panose, Phys. Rev. D **39**, 1461 (1989).

[17] F. Kruger and L. M. Sehgal, Phys. Lett. B **380**, 199 (1996) [hep-ph/9603237].

[18] B. Grinstein, D. Prijol, Phys. Rev. D **70** 114005 (2004). [arXiv:hep-ph/0404250v3].

[19] C. Bobeth, G. Hiller and D. van Dyk, JHEP **1007**, 098 (2010). [arXiv:1006.5013 [hep-ph]].

[20] S. Descotes-Genon, J. Matias, M. Ramon and J. Virto, JHEP **1301**, 048 (2013) [arXiv:1207.2753 [hep-ph]].